ACCEPTED MANUSCRIPT
Journal of Applied Physics
AIP Publishing
This is the author's peer reviewed, accepted manuscript. However, the online version of record will be different from this version once it has been copyedited and typeset.
PLEASE CITE THIS ARTICLE AS DOI: 10.1063/5.0076243

Leakage Mechanism in Ion Implantation Isolated AlGaN/GaN Heterostructures

Hao Yu[1,*], Vamsi Putcha[1], Uthayasankaran Peralagu[1], Ming Zhao[1], Sachin Yadav[1], Alireza Alian[1], Bertrand Parvais[1,2], and Nadine Collaert[1]
[1]*imec, Kapeldreef 75, Heverlee, Belgium*
[2]*Vrije Universiteit Brussels, Dept. ETRO, Belgium*
[*]hao.yu@imec.be

We report a comprehensive analysis of the leakage current mechanism in ion implantation isolation (I/I/I) regions of GaN HEMTs. We applied a three-step high-energy low-dose N I/I/I to AlGaN/AlN/GaN heterostructures. High-quality isolation is achieved with isolation sheet resistances R_{sh} in the range of 10^{13}-10^{15} Ω/sq. Analysis of isolated heterostructures with varied AlGaN or AlN thicknesses indicates common electron leakage paths at the surface of GaN. The electrostatics of the leakage path is determined by an interplay between the high densities of defects created by the I/I/I, the net sheet polarization charges between III-nitrides, and the AlGaN surface states. We find that the activation energy of the R_{sh} positively correlates with the energy level of the leakage path. The energy band diagram of the isolation region is constructed by correlating the activation energies of R_{sh} with the heterostructure electrostatics. Moreover, our study makes a novel method to estimate the net active defect density caused by the I/I/I: net active defect densities of ~2×10^{19} cm^{-3} and ~2×10^{18} cm^{-3} are extracted in the GaN and AlGaN layers, respectively.

I. Introduction

AlGaN/GaN high electron mobility transistors (HEMT) are key devices for power electronics and radio-frequency applications [1,2]. The AlGaN/GaN HEMT features a high current density and a high breakdown voltage, which enable energy efficient circuits at compact form-factors. Device isolation of HEMT is achieved with either mesa etching or ion implantation. Advantages of ion implantation isolation (I/I/I) techniques over mesa etching have been experimentally demonstrated: lower leakage and higher breakdown voltage of isolation regions are observed [3,4]. I/I/I of AlGaN/GaN heterostructures with many different ion species have been reported, such as P/He [5], Zn [6], O [7], Fe, Ar, B, N [8], C, Al [9], Kr [10].

Research on ion implantation/radiation damages in GaN has shed light upon the mechanism of the I/I/I [11–13]. Ion implantation introduces several types of defects into GaN, including point defects (Ga, N vacancies and interstitials V_{Ga}, V_N, Ga_i, and N_i), foreign ion impurities, defect complexes, local lattice disorder and amorphization [11]. These defects act as carrier trapping centres which trap carriers and pin the Fermi level away from the conduction band or the valance band of the GaN [14,15]. Without conductive free carriers the ion implanted region becomes electrically insulating. While significant lattice disorder or amorphization only occurs to heavily ion-implanted GaN, point defects and their associated complexes are the dominant defects in lightly and moderately ion-implanted GaN [11,13]. Complete annealing (recovering) of ion implantation induced damages requires temperature above 1200°C [11], which is far above the thermal budget of standard GaN device manufacturing. Therefore, the I/I/I is broadly compatible with various GaN devices.

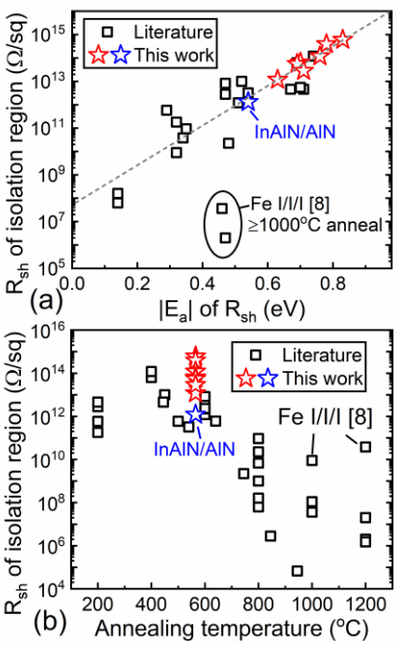

Fig. 1 Benchmarks of the R_{sh} of AlGaN/(AlN/)GaN heterostructures subjected to I/I/I. Data in literature [5–9] and in this work are summarized. Room-temperature R_{sh} is correlated with (a) its activation energy and (b) annealing temperature. The dash line in (a) is guidance for the eye. Two exception points in (a) are from heterostructures that receive particularly thermally stable Fe I/I/I and 1000°C annealing [8]. R_{sh} of $In_{0.18}Al_{0.82}N$(10 nm)/AlN(1 nm)/GaN heterostructure with I/I/I is included in (a) and (b) as a reference that shares the correlation.

confidential
This article may be downloaded for personal use only. Any other use requires prior permission of the author and AIP Publishing. This article appeared in Hao Yu, Vamsi Putcha, Uthayasankaran Peralagu, Ming Zhao, Sachin Yadav, Alireza Alian, Bertrand Parvais, Nadine Collaert; Leakage mechanism in ion implantation isolated AlGaN/GaN heterostructures. *Journal of Applied Physics* 131(3): 035701. and may be found at https://doi.org/10.1063/5.0076243.

ACCEPTED MANUSCRIPT
Journal of Applied Physics
AIP Publishing
This is the author's peer reviewed, accepted manuscript. However, the online version of record will be different from this version once it has been copyedited and typeset.
PLEASE CITE THIS ARTICLE AS DOI: 10.1063/5.0076243

The quality of the I/I/I is reflected by the sheet resistances R_{sh} of isolation regions. A R_{sh} benchmark of isolated AlGaN(/AlN)/GaN heterostructures is provided in Fig. 1. Consistent R_{sh} dependences of AlGaN/GaN heterostructures on the activation energy E_a of the R_{sh} (Fig. 1a) and on annealing temperature (Fig. 1b) have been observed among experimental AlGaN/GaN I/I/I studies [5–9]. The strong correlation between the R_{sh} and its E_a (Fig. 1a) suggests a common physical mechanism that is independent of implantation ion species. The sensitivity of the R_{sh} to annealing temperature (Fig. 1b) suggests its dependence on point defect annihilation/transformation in III nitrides [13,14,16]. Despite the high R_{sh} reported in Fig. 1 that reflects effective isolation, a full understanding of the leakage mechanism in the isolated III-N heterostructures has not been achieved. Among the few studies [17,18,34] that are dedicated to this subject, Lo *et al.* [17] and Moereke *et al.* [18] report a Poole-Frenkel path through the epitaxial buffer under high bias voltages while Zhu et al. [34] reports variable hopping conduction mechanism through localized states under such high bias voltages; it is reported in all three studies that the R_{sh} under low bias voltages is governed by ohmic mechanism, but the exact location of the ohmic path remains still unclear. Locating the ohmic leakage path in isolated heterostructures is difficult because the polarization charges and high-density defects complicate the potential profile.

This work provides understanding of the leakage mechanism in heterostructures with I/I/I. By studying isolated AlGaN/AlN/GaN with varied AlGaN and AlN thicknesses (t_{AGN} and t_{AN}, respectively), we pinpoint the ohmic leakage path at the GaN surface. Moreover, we construct the energy band diagrams for the isolation regions and estimate the net defect densities in the AlGaN and the GaN caused by the I/I/I. We have also summarized the key technological advances that contribute to the high-quality isolation.

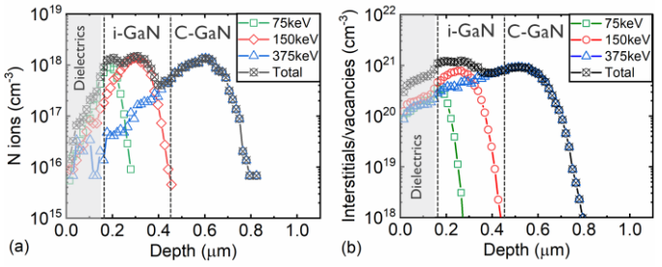

Fig. 2 Illustration of experiments for the I/I/I study. (a) N ion and (b) interstitial/vacancy profile calculated by TRIM after 3 steps of N ion implantation. Two dash lines mark GaN surface and i-GaN/C-GaN boundary respectively. The t_{AGN} and the t_{AN} are too small to vary these boundaries notably. Interstitials and vacancies have almost identical distribution.

II. EXPERIMENTAL

AlGaN/AlN/GaN structures were grown by MOCVD on high-resistivity 200 mm Si (111) substrates as described in [19]. The epitaxial buffer consists of AlN nucleation layer, AlGaN and AlGaN/AlN superlattice layers, and a 1 um thick C-doped GaN layer [20]. 300 nm unintentionally doped GaN channel layer (i-GaN) is grown on top of the buffer layers. Next, two sets of samples with varied t_{AN} or t_{AGN} were prepared: one set has a common t_{AGN} of 15 nm but a varied t_{AN} of 0, 0.5, 1, 1.5, or 2 nm; the other set has a common t_{AN} of 1 nm but a varied t_{AGN} of 4, 10, or 15 nm. The AlGaN/AlN layers were undoped. The AlGaN surfaces of all samples were *in-situ* passivated with 5 nm thick SiN [21] and *ex-situ* capped with extra 150 nm thick dielectrics. To compare with the AlGaN barrier devices, we grew a heterostructure of $In_{0.18}Al_{0.82}N$(10 nm)/AlN(1 nm)/GaN with similar cap dielectrics [20].

Next, the active regions of all samples were covered with photoresist, while the isolation regions received three steps of N ion implantation with ion energies and doses of 75 keV 8×10^{12} cm^{-2}, 150 keV 2×10^{13} cm^{-2}, and 375 keV 3×10^{13} cm^{-2}, respectively. The profile of the N ion and the associated interstitial/vacancy were calculated with the Transport of Ions in Matter (TRIM) Monte Carlo simulator in Fig. 2 [22]. The TRIM profile in Fig. 2 provides guidance on point defect distribution and density. It indicates a maximum possible carrier removal rate [36] per N ion—supposing that each point defect may effectively remove one carrier—is about 1000. But the effective carrier removal rates per N ion in experiments are much compromised due to dynamic annealing (from processing heating) induced point defect annihilation. Since the annihilation of point defects are not simulated in the TRIM [22], the point defect densities are much overestimated in Fig. 2b.

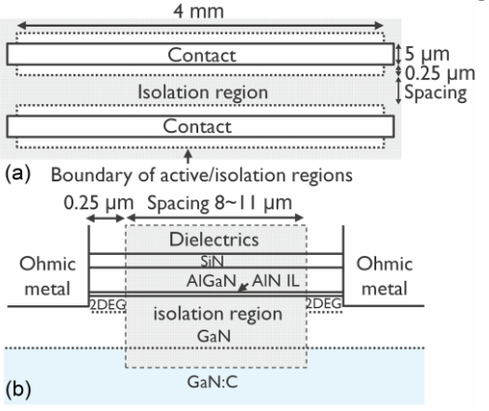

Fig. 3 (a) Schematic top view and (b) cross-sectional view of TLM structures with the I/I/I.

After the I/I/I, 4 mm wide transmission line model (TLM) structures were fabricated, as illustrated in Fig. 3. A spacing of 0.25 μm was left between the contact and the isolation region to enable ohmic contacts to 2DEG. The spacing between active regions range from 8.15 to 11.425 μm among TLM structures. There was no intentional annealing after the I/I/I. Our HEMT devices employ recessed source/drain based low-temperature contact formation [20,35]. The highest thermal budget that the isolation region received was 565ºC 90s annealing in N_2 for ohmic contact formation. The rest of the post-isolation processing of our devices, including back-end-of-line (BEOL) steps, feature low temperature below 500ºC [1, 20]. Current-voltage measurements of TLM structures were performed with a Keysight B1500A semiconductor device parameter analyzer.

III. RESULTS AND DISCUSSION

First, it is worth stressing the high room temperature R_{sh} in the range of of 10^{13}-10^{15} Ω/sq achieved in this work by N ion implantation. The R_{sh} is extracted with TLM structures (Fig. 4). As compared in Fig. 1, the R_{sh} in this work are among the

ACCEPTED MANUSCRIPT
Journal of Applied Physics
This is the author's peer reviewed, accepted manuscript. However, the online version of record will be different from this version once it has been copyedited and typeset.
PLEASE CITE THIS ARTICLE AS DOI: 10.1063/5.0076243
AIP Publishing

highest reported in literature, indicating high-quality isolation. The N I/I/I technique has been frequently studied [8,14], as the N is an intrinsic atom to the III-N. Besides (a) a proper design of the N ion implantation doses and energies (see Fig. 2), the high R_{sh} strongly benefits from (b) the low thermal budget in post-isolation processing and (c) the dielectric cap during the N ion implantation.

To achieve successful I/I/I, the combination of ion implantation and the following thermal budgets should eventually provide a sufficiently high point defect density to remove carriers but not too high a defect density to cause hopping conduction. Pearton et al. [14] have demonstrated an exemplary study how to achieve this delicate combination. This work features low-dose high-energy N ion implantation plus low post-isolation thermal budgets. Through all post-isolation processing steps, our HEMT devices employ low-temperature contact formation [20,35] and BEOL processing [1]. The 565°C 5 min contact annealing makes the dominant heating. As noted in Fig. 1b, limiting the post-isolation thermal budgets is the key to high R_{sh}, because it helps avoid point defect annihilation in the I/I/I region. In addition, the dielectric cap helps put the GaN surface at a proper depth, which helps guerantee a high point defect density near the GaN surface. As shown in Fig. 2b, the point defect density is relatively low at the exact sample surface (the dielectric surface), because high energy ions have relatively lower chances of collisions with target lattice atoms near the surface.

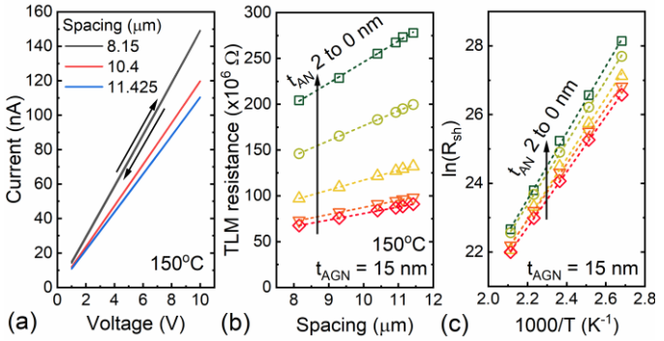

Fig. 4 Illustration of the measurement procedure on heterostructures with 15 nm AlGaN and various AlN thicknesses. (a) IV of TLM with varied spacing measured at 100-200°C. IV is linear; double-direction sweeps overlap each other. (b) R_{sh} is extracted from R_{TLM} as a function of spacing between active regions. (c) E_a of R_{sh} is extracted from the Arrhenius plot.

After demonstrating the technological keys to a high R_{sh}, we extensively analyze the leakage mechanism in the isolation region learned from experiments. The TLM resistance R_{TLM} slightly increases with bias voltages at temperature below 100°C, but the TLMs become fully ohmic (confirmed within 30 V bias voltages) within the temperature range of 100-200°C (Fig. 4a). This may be due to enhanced electron injection into the isolation region at relatively high temperature. We extract the activation energy $E_{a,Rsh}$ of R_{sh} at 100-200°C in the Arrhenius plot (Fig. 4c) by

$$R_{sh} = A\exp\left(-\frac{E_{a,Rsh}}{kT}\right) \quad (1)$$

where A is a constant, k is the Boltzmann constant, T is temperature. (The activation energies of the 2DEG density N_{sh} and mobility μ in later texts are defined in a similar way with R_{sh}.) As shown in Fig. 5, the R_{sh} and the $|E_{a,Rsh}|$ decrease with the t_{AN} but increase with the t_{AGN}. These $t_{A(G)N}$ dependences will be explained from the band diagrams of the isolated heterostructures which are presented in the next section.

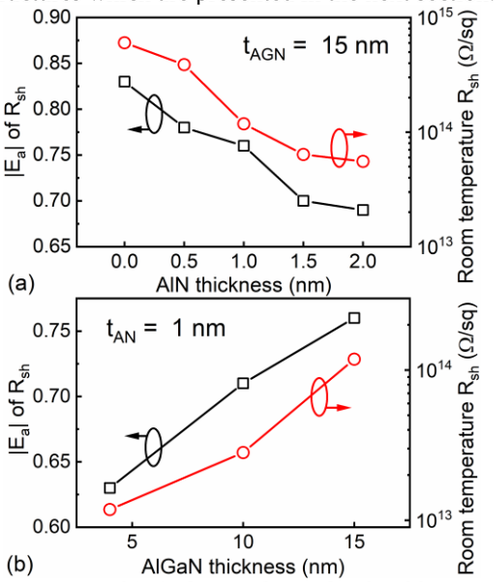

Fig. 5 Experimental $|E_a|$ of R_{sh} and R_{sh} of isolated heterostructures at room temperature as a function of (a) t_{AN} or (b) t_{AGN}.

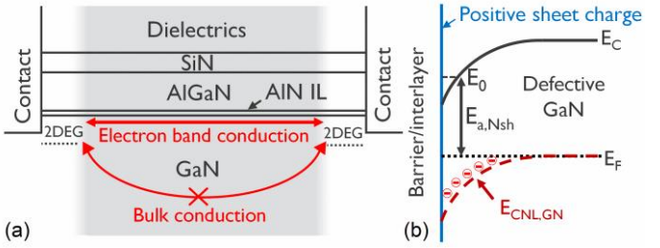

Fig. 6 Schematics illustrating leakage mechanism in GaN heterostructures. (a) Surface leakage path vs bulk leakage path in TLM. (b) Energy band diagram of GaN surface showing polarization charge induced band bending.

The TLM characteristics help distinguish the dominant leakage mechanism in isolated heterostructures (Fig. 6). The ohmic behavior of the isolated heterostructures under a relatively low electric field (<10^5 V/cm) is consistent with previous studies [17,18]. The ohmic IV excludes hopping-conduction-via-defect-site as the dominant conduction mechanism [14], under which the current would have exponential dependence on the electric field [23]. Rather, the ohmic behavior suggests band conduction of free carriers. Furthermore, the conductive free carriers are electrons rather than holes—otherwise supplying the minority hole carriers from 2DEG regions into the isolation region (see Fig. 6a) would lead to significant non-linear IV of the TLM. In addition, the distinct R_{sh} of heterostructures with varied $t_{A(G)N}$ (Fig. 5) suggest against dominant conduction via the GaN bulk. This is because the GaN bulk potentials defined by the same I/I/I processing are similar between various heterostructures (see Fig. 3a-b, where the small t_{AGN} and t_{AN} are negligible compared to the depth of defect distribution) and would result in similar conduction in magnitudes via the bulk. In summary, the leakage in the isolation region is dominated by the electrons via the GaN surface conduction band (Fig. 6).

ACCEPTED MANUSCRIPT
Journal of Applied Physics
AIP Publishing
This is the author's peer reviewed, accepted manuscript. However, the online version of record will be different from this version once it has been copyedited and typeset.
PLEASE CITE THIS ARTICLE AS DOI: 10.1063/5.0076243

Under the ohmic regime, the R_{sh} of electron band conduction at the GaN surface has the following expression [24]

$$R_{sh} = \frac{1}{q\mu N_{sh}} = \frac{1}{q\mu D_{C,GN} kT \exp\left(-\frac{E_0 - E_F}{kT}\right)} = \frac{1}{q\mu D_{C,GN} kT \exp\left(-\frac{E_{a,Nsh}}{kT}\right)} \quad (2)$$

where N_{sh} is the sheet electron density in the leakage channel, μ is the electron mobility, $D_{C,GN}$ is the 2D conduction band effective density of states of GaN, E_0 is the first sub-band in the conduction band of GaN due to quantization, $E_{a,Nsh}$ is the activation energy of N_{sh}. $D_{C,GN}$ and E_0 are introduced in (2), because the net polarization charges induced high electric fields near the GaN surface cause quantization in the conduction band [24] (the upper sub-bands in the GaN well are neglected due to the high surface electric field). This high electric field is evidenced in simulation in the next section. With (2), the correlations between $E_{a,Rsh}$ and R_{sh} in Fig. 1a and Fig. 5 are qualitatively understood: the higher the energy level of the leakage path is at the GaN surface, the fewer carriers present in the path, and the higher R_{sh} obtained.

Further, formation of the leakage path at the GaN surface of isolated AlGaN/AlN/GaN heterostructures is theoretically expected. The path forms due to interaction between interfacial polarization charges and the GaN bulk defects caused by the I/I/I. Net positive sheet charges locate at the Al(Ga)N/GaN interface due to the differences in spontaneous and piezoelectric polarization charges between the Al(Ga)N and the GaN [25]. The positive polarization sheet charges attract negative charges from the defective GaN bulk. This is accompanied by downward bending of GaN energy bands, as illustrated in Fig. 6b: the net charges are negative in the band bending region, as the Fermi level E_F is above the charge neutrality level $E_{CNL,GN}$. As a result, the band bending induces leakage paths at relatively low energy levels at the GaN surface compared to the conduction band minimum E_C in the GaN bulk.

The above leakage path formation mechanism is not unique to the AlGaN/GaN heterostructure but also applies to other wurtzite III-N stacks. In Fig. 1a, isolated InAlN/AlN/GaN heterostructure shares the same R_{sh}-$E_{a,Rsh}$ correlations with the AlGaN/(AlN/)GaN ones. The relatively low $E_{a,Rsh}$ and the R_{sh} of the InAlN/AlN/GaN sample are consistent with the fact that the net polarization charge density between the $In_{0.18}Al_{0.82}N$/GaN is almost two times as high as that between the $Al_{0.25}Ga_{0.75}N$/GaN [25]. This causes stronger GaN band bending and thus a lower $E_{a,Rsh}$ of the isolated InAlN/AlN/GaN heterostructure than those of the AlGaN/AlN/GaN. Clearly, the aforementioned leakage mechanism in isolated heterostructures further applies to other piezoelectric systems.

The discussion in this section has laid foundations for understanding the electrostatics of isolated AlGaN/AlN/GaN heterostructures. In the next section, exploiting extra information contained in the $E_{a,Rsh}$-t_{AN} and $E_{a,Rsh}$-t_{AGN} relationships in Fig. 5, we will reconstruct the full energy diagrams of the isolated heterostructure and estimate defect densities in the AlGaN and the GaN.

IV. MODELING

Detailed modeling of defective heterostructures is helpful for understanding the electrostatics, quantifying charge densities, evaluating processing conditions, and learning reliability concerns [26]. In addition, in GaN-on-Si HEMTs, knowledge of the electrostatic modification by the I/I/I is crucial to understanding its impact on Si substrate RF losses and harmonic distortion [27]. But in an isolated heterostructure, the multiple layers and many defect types make complex electrostatics. We confront the challenge by simplifying the scenario and applying available knowledge in literature.

In undoped AlGaN/Al/GaN heterostructures, an increased t_{AN} increases the 2DEG density [28,29]. This is theoretically explained by an interplay between the polarization charges σ, the surface state charges of the AlGaN Q_{SS}, and the 2DEG [29,30]. As for isolated heterostructures, where the 2DEG density is small, the electrostatics are controlled by the σ, the Q_{SS}, and the bulk defect charges in AlGaN/AlN/GaN induced by the I/I/I. With presence of multiple types of bulk defects exist, we reduce the simulation complexity by using charge neutrality level E_{CNL} and net bulk defect density n_{net} to describe the electrostatics. Even with this simplification, three sets of E_{CNL} and n_{net} are still needed for the AlGaN, the AlN, and the GaN respectively to describe the electrostatics near the GaN surface. The unknowns outnumber the variables that can be accurately extracted from the two curves in Fig. 5. Therefore, we focus on net defect densities in the AlGaN and the GaN, and make the following simplification assumptions:

(i) no implant damage in the AlN (considering that the t_{AN} of 0-2 nm is small);

(ii) a uniform $n_{n,AGN}$ of the AlGaN and a uniform $n_{n,GN}$ near the GaN surface (considering that the t_{AGN} and the leakage path are small compared to the ion implantation depth, see Fig. 2b);

(iii) no net charges in cap dielectrics;

(iv) the bulk defects are discrete in energies;

(v) the $E_{CNL,GN}$ of GaN is 0.8~1.0 eV below the bulk GaN conduction band minimum $E_{C,GN}$;

(vi) strain is preserved after the I/I/I plus the 565°C ohmic annealing (the lattice of heterostructures that receive comparable I/I/I recovers mostly after 400-800°C [9]).

The assumption (iv) has an important implication: in the defective GaN bulk at equilibrium, only the discrete bulk defects with energy levels closest to the $E_{CNL,GN}$ may vary the trapping status as a function of the depth in the band bending region (see Fig. 6b for instance). The other defects whose energies differ much from E_F and $E_{CNL,GN}$ are either constantly filled or constantly emptied.

The assumption (v) is justified by experimental observations [14,15,31]. The E_F pinning is dominated by the interstitials—N_i^- acceptors and Ga_i^{++} double donors, which locate around 1.0 eV and 0.8 eV below $E_{C,GN}$, respectively [13]. In the isolated heterostructures of this work, the point defects induced by the I/I/I are preserved in a large amount because of the <600°C thermal budget in fabrication [13,16]. This is also supported by observations of the R_{sh}-annealing dependence in Fig. 1b—the high R_{sh} induced by the populated point defects remain with <600°C annealing.

Together with these assumptions, the parameters in Table I were used to simulate the isolated heterostructures. Aligning

ACCEPTED MANUSCRIPT
Journal of Applied Physics
This is the author's peer reviewed, accepted manuscript. However, the online version of record will be different from this version once it has been copyedited and typeset.
PLEASE CITE THIS ARTICLE AS DOI: 10.1063/5.0076243
AIP Publishing

with the assumption (iv) and (v), the $E_{1,GN}$ and the $E_{2,GN}$ mimic the N_i^- and the Ga_i^{++} energy levels in the GaN [13] and establish the presumed $E_{CNL,GN}$. We use the $E_{3,AGN}$ to describe the defects induced net charging in the AlGaN. As marked in Table I, only four unkowns remain in our simulation: the densities of $E_{1,GN}$, $E_{2,GN}$, and $E_{3,AGN}$, and the polarity/the energy level of the $E_{3,AGN}$. The number of variables is small enough for meaningful parameter extraction.

TABLE I. Parameters in simulation of isolated heterostructures

Symbol	Description	Value
σ_{GN}	Polarization charge of GaN	2.13×10^{13} q/cm^{-2} [25][a]
σ_{AGN}	Polarization charge of $Al_{0.25}Ga_{0.75}N$	3.56×10^{13} q/cm^2 [29][b]
σ_{AN}	Polarization charge of AlN	7.03×10^{13} q/cm^2 [29][b]
D_{SS}	AlGaN surface state density (passivated by *in-situ* SiN)	2.9×10^{12} /(eV·cm) [29][b]
$E_{CNL,S}$	Charge neutrality level of the AlGaN surface	$E_{C,AGNS}$-0.95 eV [29][b,c]
$E_{a,\mu}$	Activation energy of the electron mobility with ion implantation damage	0.17 eV [33][d]
$E_{1,GN}$	Presumed acceptor defect in bulk GaN	$E_{C,GN}$-1.0 eV [13]; Density to be extracted
$E_{2,GN}$	Presumed donor defect in bulk GaN	$E_{C,GN}$-0.8 eV [13]; Density to be extracted
$E_{3,AGN}$	Presumed defect in bulk AlGaN; polarity to be extracted	Energy level and density to be extracted

[a]q is the elementary charge
[b]Experimentally extracted values from undoped heterostructures in our previous experiments
[c]$E_{C,AGNS}$ is the AlGaN conduction band minimum energy at the surface
[d]Value from experiments with He ion implanted GaN [32]

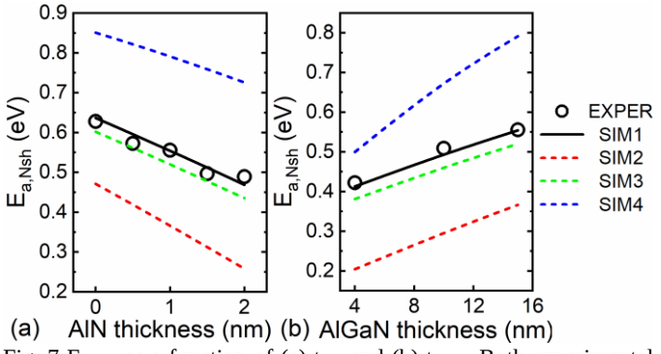

Fig. 7 $E_{a,Nsh}$ as a function of (a) t_{AN} and (b) t_{AGN}. Both experimental and simulated data are included. Simulation SIM1-4 applies varied input defect densities, listed in TABLE II. SIM1 aims to fit experimental data; SIM2-4 serve as comparison.

TABLE II. Input defect densities in simulation

Run	Acceptor $E_{1,GN}$ (cm^{-3})	Donor $E_{2,GN}$ (cm^{-3})	Acceptor $E_{3,AGN}$ (cm^{-3})
SIM1	1.9×10^{19}	3.0×10^{19}	1.9×10^{18}
SIM2	1.5×10^{19}	3.0×10^{19}	1.9×10^{18}
SIM3	1.9×10^{19}	1.0×10^{20}	1.9×10^{18}
SIM4	1.9×10^{19}	3.0×10^{19}	5.0×10^{18}

Since the energy level of the leakage path at the GaN surface is apparently linked to the $E_{a,Nsh}$ rather than the $E_{a,Rsh}$ (see Fig. 6b), we derive $E_{a,Nsh}$-$t_{A(G)N}$ dependences in Fig. 7 before curve fitting. The $E_{a,Nsh}$ is derived by sorting the T dependence of R_{sh}, N_{sh}, and μ in (2)

$$E_{a,Nsh} = -E'_{a,Rsh} - E_{a,\mu} \quad (3)$$

where the $E'_{a,Rsh}$ is the activation energy of the R_{sh}·T. Small positive $E_{a,\mu}$ (<200 meV) have been experimentally reported in defective GaN because of the high defect density induced lattice potential fluctuation [32,33]. We assume the same $E_{a,\mu}$ in Table I for all samples, because impurity scattering dominates μ degradation in the defective GaN, and the total defect densities created by the same I/I/I process are similar between samples. The trend of the $E_{a,Nsh}$-$t_{A(G)N}$ curves in Fig. 7 follows closely that of the $E_{a,Rsh}$-$t_{A(G)N}$ curves in Fig. 5.

Next to the scenario and parameter setup, the electrostatics of the isolated AlGaN/AlN/GaN heterostructures at equilibrium are simulated obeying criteria of charge neutrality and Kirchhoff's voltage law. A proper combination of the $E_{1,GN}$, $E_{2,GN}$, and $E_{3,AGN}$—the SIM1 condition in TABLE II—enables good fitting of $E_{a,Nsh}$-$t_{A(G)N}$ curves in Fig. 7. The densities of the $E_{1,GN}$, $E_{2,GN}$, and $E_{3,AGN}$ are 1.9×10^{19} cm^{-3}, 3×10^{19} cm^{-3}, and 1.9×10^{18} cm^{-3}, respectively. The $E_{3,AGN}$ is of the acceptor type and locates in the lower half of the band gap of the AlGaN. In Fig.7, we show simulated energy band diagrams of the heterostructures with parameters that fit the experimental $E_{a,Nsh}$-$t_{A(G)N}$ curves in Fig. 7. The energy band diagrams help clearly interpret how R_{sh} and $E_{a,Nsh}$ vary with the t_{AN} and the t_{AGN}.

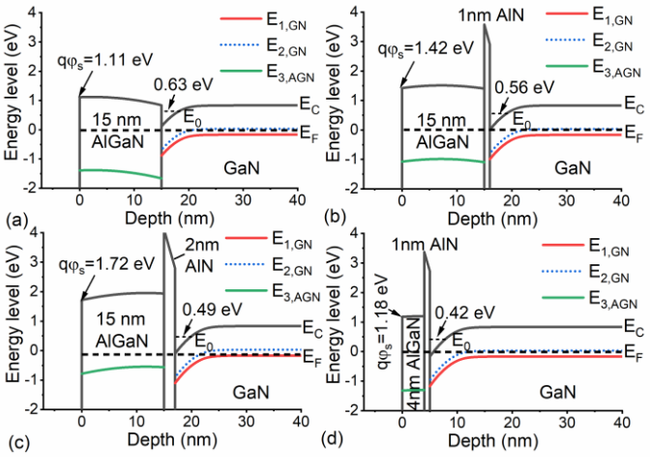

Fig. 8 Simulated energy band diagrams of (a) 15 nm AlGaN/GaN, (b) 15 nm AlGaN/1 nm AlN/GaN, (c) 15 nm AlGaN/2 nm AlN/GaN, (d) 15 nm AlGaN/1 nm AlN/GaN. The input densities of $E_{1,GN}$, $E_{2,GN}$, and $E_{3,AGN}$ apply the SIMU1 condition in TABLE II. Energies of AlGaN surface potential $q\varphi_s$ and sub-band E_0 of GaN conduction band are marked in plots.

The t_{AN} impact is clarified by comparing Fig. 8a-c. With a much higher σ_{AN} than the σ_{AGN} and the σ_{GN} [25], an increased t_{AN} adds the effective band offset between the AlGaN and the GaN [27,28]. Effectively, the energy band of the AlGaN is shifted up with respect to the E_F. This makes the net charges in the bulk AlGaN, and at the AlGaN surface, more positive, which in turn induces more negative charges from the GaN bulk, i.e. enhanced band bending at the GaN surface. Therefore, an increased t_{AN} enhances GaN surface band bending, decreases $E_{a,Nsh}$ (Fig 6b), and thus decreases the R_{sh} (Fig. 5b).

The t_{AGN} impact is clarified by comparing Fig. 8b and Fig. 8d. A monotonous increase of increase of $E_{a,Nsh}$—enhanced GaN surface band bending—with the t_{AGN} (Fig. 8b) indicates that the net bulk defect charge in the AlGaN is negative in polarity (when E_F is around 1~1.5 eV below the E_C of the AlGaN according to Fig. 8b and Fig. 8d). With net negative

ACCEPTED MANUSCRIPT
Journal of Applied Physics
AIP Publishing
This is the author's peer reviewed, accepted manuscript. However, the online version of record will be different from this version once it has been copyedited and typeset.
PLEASE CITE THIS ARTICLE AS DOI: 10.1063/5.0076243

charges in the bulk AlGaN, an increased t_{AGN} adds negative charges to the system; both the AlGaN surface charges and the GaN bulk charges get more positive to maintain charge neutrality in the system. Therefore, an increased t_{AGN} reduces GaN surface band bending, increases $E_{a,Nsh}$ (Fig 6b), and thus decreases the R_{sh} (Fig. 4b). With the available data and knowledge in literature, we cannot determine the exact energy level of the dominant acceptors that provide negative charges in the AlGaN. Therefore, we arbitrarily assume the acceptor $E_{3,AGN}$ at 2.5 eV below the E_C of the AlGaN (see Fig. 7), so that the $E_{3,AGN}$ are constantly ionized in all simulation scenarios.

The good fitting of $E_{a,Nsh}$-$t_{A(G)N}$ curves is accomplished with a proper combination of densities of the states $E_{1,GN}$, $E_{2,GN}$, and $E_{3,AGN}$—as the SIM1 condition in TABLE II. Although the $E_{1,GN}$, $E_{2,GN}$, and $E_{3,AGN}$ are imaginary trapping states, they help well reproduce electrostatics of the isolated heterostructures. The density extraction that is based on $E_{a,Nsh}$-$t_{A(G)N}$ fitting is very sensitive for $E_{1,GN}$ and $E_{3,AGN}$ (see Fig. 7). This is understood since the acceptor $E_{1,GN}$ represents net negative charges that establish the GaN surface band bending, and the acceptor $E_{3,AGN}$ represents net negative charges in the AlGaN. However, the density extraction is not sensitive to the $E_{2,GN}$, because the donor $E_{2,GN}$ is neutral in the band bending region; the main role of the $E_{2,GN}$ in this simulation is to compensate the $E_{1,GN}$ in the GaN bulk and establish the frequently observed $E_{CNL,GN}$ [14,15,31]. Therefore, the $E_{1,GN}$ and the $E_{3,AGN}$ provide good references to estimate the net defect densities created by the I/I/I in the GaN and the AlGaN. Since the $E_{1,GN}$ mimic the N_i^- interstitials in the GaN [13], we speculate that the N_i^- interstitials play a crucial role in isolation of the GaN based heterostructures that do not receive high-temperature annealing.

To our knowledge, only few quantitative methods exist to measure or estimate (point) defect densities in highly defective III-N. The TRIM simulation in Fig. 1b provides useful large-range distribution of the point defects caused by the I/I/I. But the point defect density is much overestimated in the TRIM simulation without considering dynamic annealing [22]. The $E_{a,Nsh}$-$t_{A(G)N}$ fitting method in this work provides a novel way to estimate the realistic *net* defect densities in the defective III-N.

V. CONCLUSIONS

We demonstrate high-quality N ion implantation isolation (I/I/I) of AlGaN/AlN/GaN heterostructures. The sheet resistances R_{sh} of isolated heterostructures are as high as 10^{13}-10^{15} Ω/sq at room temperature, among the highest reported to date. The high R_{sh} benefits from processing advantages including a key low thermal budget in device fabrication.

For the first time, we elucidate the underlying leakage mechanism in isolated GaN based heterostructures. The leakage occurs via an ohmic path of electrons at the GaN surface. The ohmic path forms with downwards band bending of the GaN conduction band near the GaN surface. The band bending is caused by interaction between the net positive polarization charge at the Al(Ga)N/GaN surface and the high-density bulk defects in the GaN induced by the I/I/I. We use isolated heterostructures with varied AlGaN and AlN thicknesses (t_{AGN} and t_{AN}) to help clarify the leakage mechanism. We observe that the R_{sh} and the absolute activation energy of the R_{sh}—the $|E_{a,Rsh}|$—decrease with the t_{AN} but increase with the t_{AGN}. The aforementioned leakage mechanism help well interpret the R_{sh} and $|E_{a,Rsh}|$ dependences on the $t_{A(G)N}$. Moreover, we construct the energy band diagrams for the heterostructures, which clearly illustrate the electrostatics of the isolated heterostructures. By fitting experimental $|E_{a,Rsh}|$ with varied $t_{A(G)N}$, we manage to estimate the net defect densities caused by the I/I/I, which are ~2×10^{19} cm^{-3} and ~2×10^{18} cm^{-3} in the GaN and in the AlGaN, respectively. We find a common R_{sh}-$|E_{a,Rsh}|$ dependence of isolated heterostructures among this work and several other studies in literature, suggesting that the leakage mechanism reported in this work is widely applicable.

Data availability

The data that supports the findings of this study are available within the article.

REFERENCES

[1] B. Parvais, A. Alian, U. Peralagu, R. Rodriguez, S. Yadav, A. Khaled, R. Y. Elkashlan, V. Putcha, A. Sibaja-Hernandez, M. Zhao, P. Wambacq, N. Collaert, and N. Waldron, *GaN-on-Si Mm-Wave RF Devices Integrated in a 200mm CMOS Compatible 3-Level Cu BEOL*, in *Technical Digest - International Electron Devices Meeting, IEDM* (2020), pp. 155–158.

[2] M. Micovic, D. F. Brown, D. Regan, J. Wong, Y. Tang, F. Herrault, D. Santos, S. D. Burnham, J. Tai, E. Prophet, I. Khalaf, C. McGuire, H. Bracamontes, H. Fung, A. K. Kurdoghlian, and A. Schmitz, *High Frequency GaN HEMTs for RF MMIC Applications*, in *IEEE International Electron Devices Meeting* (IEEE, 2016), pp. 59–62.

[3] H. Sun, A. R. Alt, S. Tirelli, D. Marti, H. Benedickter, E. Piner, and C. R. Bolognesi, *Nanometric AlGaN/GaN HEMT Performance with Implant or Mesa Isolation*, IEEE Electron Device Lett. **32**, 1056 (2011).

[4] M. Sun, H. S. Lee, B. Lu, D. Piedra, and T. Palacios, *Comparative Breakdown Study of Mesa- and Ion-Implantation-Isolated AlGaN/GaN High-Electron-Mobility Transistors on Si Substrate*, Appl. Phys. Express **5**, (2012).

[5] G. Hanington, Y. M. Hsin, Q. Z. Liu, P. M. Asbeck, S. S. Lau, M. Asif Khan, J. W. Yang, and Q. Chen, *P/He Ion Implant Isolation Technology for AlGaN/GaN HFETs*, Electron. Lett. **34**, 193 (1998).

[6] T. Oishi, N. Miura, M. Suita, T. Nanjo, Y. Abe, T. Ozeki, H. Ishikawa, T. Egawa, and T. Jimbo, *Highly Resistive GaN Layers Formed by Ion Implantation of Zn along the c Axis*, J. Appl. Phys. **94**, 1662 (2003).

[7] J. Y. Shiu, J. C. Huang, V. Desmaris, C. T. Chang, C. Y. Lu, K. Kumakura, T. Makimoto, H. Zirath, N. Rorsman, and E. Y. Chang, *Oxygen Ion Implantation Isolation Planar Process for AlGaN/GaN HEMTs*, IEEE Electron Device Lett. **28**, 476 (2007).

[8] H. Umeda, T. Takizawa, Y. Anda, T. Ueda, and T. Tanaka, *High-Voltage Isolation Technique Using Fe Ion Implantation for Monolithic Integration of AlGaN/GaN Transistors*, IEEE Trans. Electron Devices **60**, 771 (2013).

[9] A. Taube, E. Kamińska, M. Kozubal, J. Kaczmarski, W. Wojtasiak, J. Jasiński, M. A. Borysiewicz, M. Ekielski, M. Juchniewicz, J. Grochowski, M. Myśliwiec, E. Dynowska, A. Barcz, P. Prystawko, M. Zając, R. Kucharski, and A. Piotrowska, *Ion Implantation for Isolation of AlGaN/GaN HEMTs Using C or Al*, Phys. Status Solidi Appl. Mater. Sci. **212**, 1162 (2015).

[10] S. Arulkumaran, K. Ranjan, G. I. Ng, J. Kennedy, P. P. Murmu, T. N. Bhat, and S. Tripathy, *Thermally Stable Device Isolation by Inert Gas Heavy Ion Implantation in AlGaN/GaN HEMTs on Si*, J. Vac. Sci. Technol. B, Nanotechnol. Microelectron. Mater. Process. Meas. Phenom. **34**, 042203 (2016).

[11] S. O. Kucheyev, J. S. Williams, J. Zou, C. Jagadish, and G. Li, *Ion Implantation into GaN*, Mater. Sci. Eng. R **33**, 51 (2001).

[12] S. J. Pearton, F. Ren, E. Patrick, M. E. Law, and A. Y. Polyakov, *Review—Ionizing Radiation Damage Effects on GaN Devices*, ECS J. Solid State Sci. Technol. **5**, Q35 (2016).

[13] A. Y. Polyakov, S. J. Pearton, P. Frenzer, F. Ren, L. Liu, and J. Kim, *Radiation Effects in GaN Materials and Devices*, J. Mater.

ACCEPTED MANUSCRIPT
Journal of Applied Physics
AIP Publishing
This is the author's peer reviewed, accepted manuscript. However, the online version of record will be different from this version once it has been copyedited and typeset.
PLEASE CITE THIS ARTICLE AS DOI: 10.1063/5.0076243

Chem. C **1**, 877 (2013).

[14] S. J. Pearton, C. B. Vartuli, J. C. Zolper, C. Yuan, and R. A. Stall, *Ion Implantation Doping and Isolation of GaN*, Appl. Phys. Lett. **67**, 1435 (1995).

[15] A. Y. Polyakov, N. B. Smirnov, A. V. Govorkov, A. V. Markov, N. G. Kolin, D. I. Merkurisov, V. M. Boiko, K. D. Shcherbatchev, V. T. Bublik, M. I. Voronova, I. H. Lee, C. R. Lee, S. J. Pearton, A. Dabirian, and A. V. Osinsky, *Fermi Level Pinning in Heavily Neutron-Irradiated GaN*, J. Appl. Phys. **100**, (2006).

[16] C. Ronning, M. Dalmer, M. Uhrmacher, M. Restle, U. Vetter, L. Ziegeler, H. Hofsäss, T. Gehrke, K. Järrendahl, and R. F. Davis, *Ion Implanted Dopants in GaN and AlN: Lattice Sites, Annealing Behavior, and Defect Recovery*, J. Appl. Phys. **87**, 2149 (2000).

[17] J. Moereke, E. Morvan, W. Vandendaele, F. Allain, A. Torres, M. Charles, and M. Plissonnier, *Leakage Current Paths in Isolated AlGaN/GaN Heterostructures*, IEEE Trans. Semicond. Manuf. **29**, 363 (2016).

[18] C. F. Lo, T. S. Kang, L. Liu, C. Y. Chang, S. J. Pearton, I. I. Kravchenko, O. Laboutin, J. W. Johnson, and F. Ren, *Isolation Blocking Voltage of Nitrogen Ion-Implanted AlGaN/GaN High Electron Mobility Transistor Structure*, Appl. Phys. Lett. **97**, 6 (2010).

[19] M. Zhao, Y. Saripalli, P. K. Kandaswamy, H. Liang, A. Firrincieli, S. Decoutere, and E. Vancoille, *Growth and Characterization of DH-HEMT Structures with Various AlGaN Barriers and AlN Interlayers on 200 Mm Si(111) Substrates*, Phys. Status Solidi Curr. Top. Solid State Phys. **11**, 446 (2014).

[20] U. Peralagu, B. De Jaeger, D. M. Fleetwood, P. Wambacq, M. Zhao, B. Parvais, N. Waldron, N. Collaert, A. Alian, V. Putcha, A. Khaled, R. Rodriguez, A. Sibaja-Hernandez, S. Chang, E. Simoen, and S. E. Zhao, *CMOS-Compatible GaN-Based Devices on 200mm-Si for RF Applications: Integration and Performance*, in *International Electron Devices Meeting, IEDM* (2019), pp. 398–401.

[21] J. Derluyn, S. Boeykens, K. Cheng, R. Vandersmissen, J. Das, W. Ruythooren, S. Degroote, M. R. Leys, M. Germain, and G. Borghs, *Improvement of AlGaNGaN High Electron Mobility Transistor Structures by in Situ Deposition of a Si3N4 Surface Layer*, J. Appl. Phys. **98**, 054501 (2005).

[22] J. F. Ziegler, M. D. Ziegler, and J. P. Biersack, *SRIM - The Stopping and Range of Ions in Matter (2010)*, Nucl. Instruments Methods Phys. Res. Sect. B Beam Interact. with Mater. Atoms **268**, 1818 (2010).

[23] V. F. Gantmakher, *Electrons and Disorder in Solids*, 1st ed., Vol. 9780198567 (Oxford University Press, 2005).

[24] J. H. Davies, *The Physics of Low-Dimensional Semiconductors: An Intorduction* (Cambridge University Press, 1998).

[25] O. Ambacher, J. Majewski, C. Miskys, A. Link, M. Hermann, M. Eickhoff, M. Stutzmann, F. Bernardini, V. Fiorentini, V. Tilak, B. Schaff, and L. F. Eastman, *Pyroelectric Properties of Al(In)GaN/GaN Hetero- and Quantum Well Structures*, J. Phys. Condens. Matter **14**, 3399 (2002).

[26] L. Lv, X. Ma, H. Xi, L. Liu, Y. Cao, J. Zhang, H. Shan, and Y. Hao, *Theoretical Analysis of Proton Irradiation Effects on AlGaN/GaN High-Electron-Mobility Transistors*, J. Vac. Sci. Technol. B, Nanotechnol. Microelectron. Mater. Process. Meas. Phenom. **33**, 051212 (2015).

[27] S. Yadav, P. Cardinael, M. Zhao, K. Vondkar, A. Khaled, R. Rodriguez, B. Vermeersch, S. Makovejev, E. Ekoga, A. Pottrain, N. Waldron, N. Collaert, *Substrate RF losses and non-linearities in GaN-on-Si HEMT technology*, in *Technical Digest - International Electron Devices Meeting, IEDM* (2020), pp. 8.2.1-8.2.4.

[28] L. Shen, S. Heikman, B. Moran, R. Coffie, N. Q. Zhang, D. Buttari, I. P. Smorchkova, S. Keller, S. P. DenBaars, and U. K. Mishra, *AlGaN/AlN/GaN High-Power Microwave HEMT*, IEEE Electron Device Lett. **22**, 457 (2001).

[29] H. Yu, A. Alian, U. Peralagu, M. Zhao, N. Waldron, B. Parvais, and N. Collaert, *Surface State Spectrum of AlGaN/AlN/GaN Extracted from Static Equilibrium Electrostatics*, IEEE Trans. Electron Devices, **68**, 5559, (2021).

[30] N. Goyal and T. A. Fjeldly, *Analytical Modeling of AlGaN/AlN/GaN Heterostructures Including Effects of Distributed Surface Donor States*, Appl. Phys. Lett. **105**, (2014).

[31] A. Y. Polyakov, N. B. Smirnov, A. V. Govorkov, N. G. Kolin, D. I. Merkurisov, V. M. Boiko, A. V. Korulin, and S. J. Pearton, *Neutron Transmutation Doping Effects in GaN*, J. Vac. Sci. Technol. B **28**, 608 (2010).

[32] M. Fehrer, S. Einfeldt, U. Birkle, T. Gollnik, and D. Hommel, *Impact of Defects on the Carrier Transport in GaN*, J. Cryst. Growth **189**–**190**, 763 (1998).

[33] J. Salzman, C. Uzan-Saguy, R. Kalish, V. Richter, and B. Meyler, *Thermally Activated Electrical Conductivity in Thin GaN Epitaxial Films*, Appl. Phys. Lett. **76**, 1431 (2000).

[34] J. Zhu, Y. Zhang, M. J. Uren, S. Liu, P. Wang, M. Mi, B. Hou, L. Yang, M. Kuball, X. Ma, and Y. Hao, *Variable range hopping mechanism and modeling of isolation leakage current in GaN-based high-electron-mobility transistors*, Appl. Phys. Lett., **116**, 222101 (2020).

[35] A. Firrincieli, B. De Jaeger, S. You, D. Wellekens, M. Van Hove, and S. Decoutere, *Au-free low temperature ohmic contacts for AlGaN/GaN power devices on 200 mm Si substrates*, Jpn J. Appl. Phys., **53**, 04EF01 (2014).

[36] S. J. Pearton, *Ion implantation for isolation of III-V semiconductors*, Mater. Sci. Rep. **4**, 313 (1991).

ACCEPTED MANUSCRIPT

Journal of Applied Physics

This is the author's peer reviewed, accepted manuscript. However, the online version of record will be different from this version once it has been copyedited and typeset.

PLEASE CITE THIS ARTICLE AS DOI: 10.1063/1.5143243

AIP Publishing

Journal of Applied Physics

ACCEPTED MANUSCRIPT

This is the author's peer reviewed, accepted manuscript. However, the online version of record will be different from this version once it has been copyedited and typeset.

PLEASE CITE THIS ARTICLE AS DOI: 10.1063/5.0076243

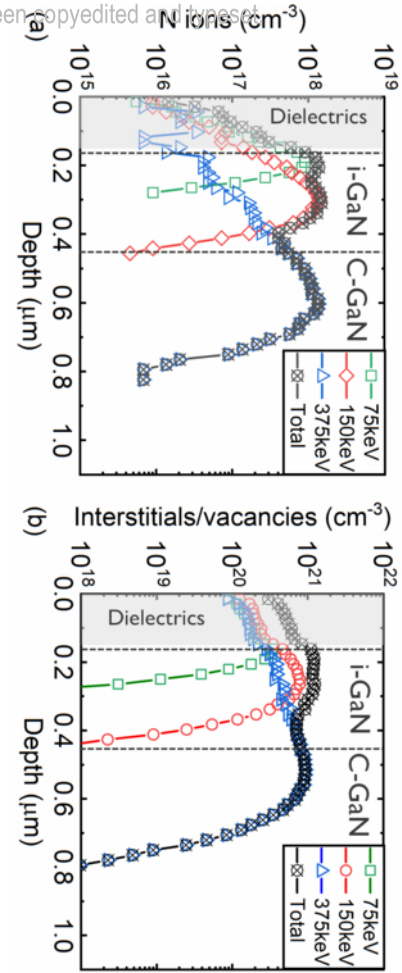

ACCEPTED MANUSCRIPT

Journal of Applied Physics

This is the author's peer reviewed, accepted manuscript. However, the online version of record will be different from this version once it has been copyedited and typeset.
PLEASE CITE THIS ARTICLE AS DOI: 10.1063/5.0076243

AIP Publishing

Journal of Applied Physics

ACCEPTED MANUSCRIPT

This is the author's peer reviewed, accepted manuscript. However, the online version of record will be different from this version once it has been copyedited and typeset.

PLEASE CITE THIS ARTICLE AS DOI: 10.1063/5.0076243

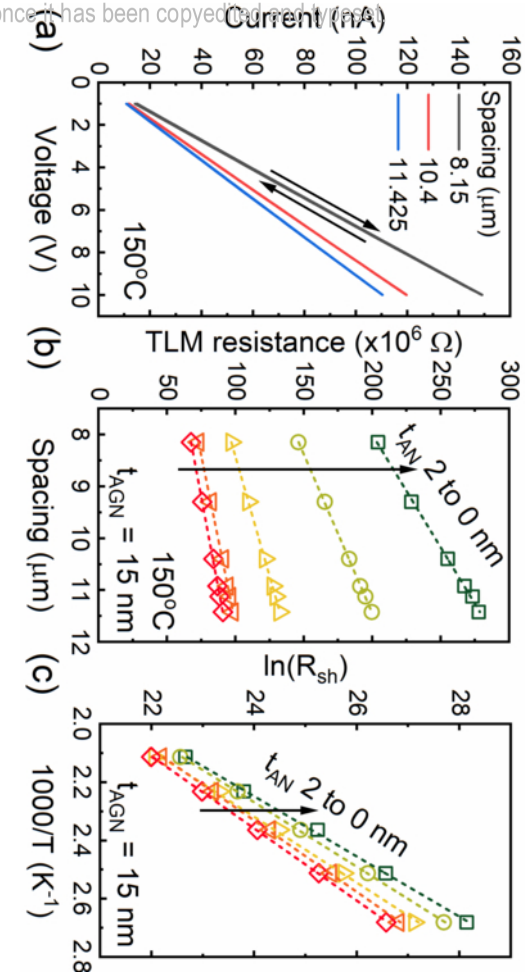

AIP Publishing

Journal of Applied Physics

ACCEPTED MANUSCRIPT

This is the author's peer reviewed, accepted manuscript. However, the online version of record will be different from this version once it has been copyedited and typeset.
PLEASE CITE THIS ARTICLE AS DOI: 10.1063/1.5076245

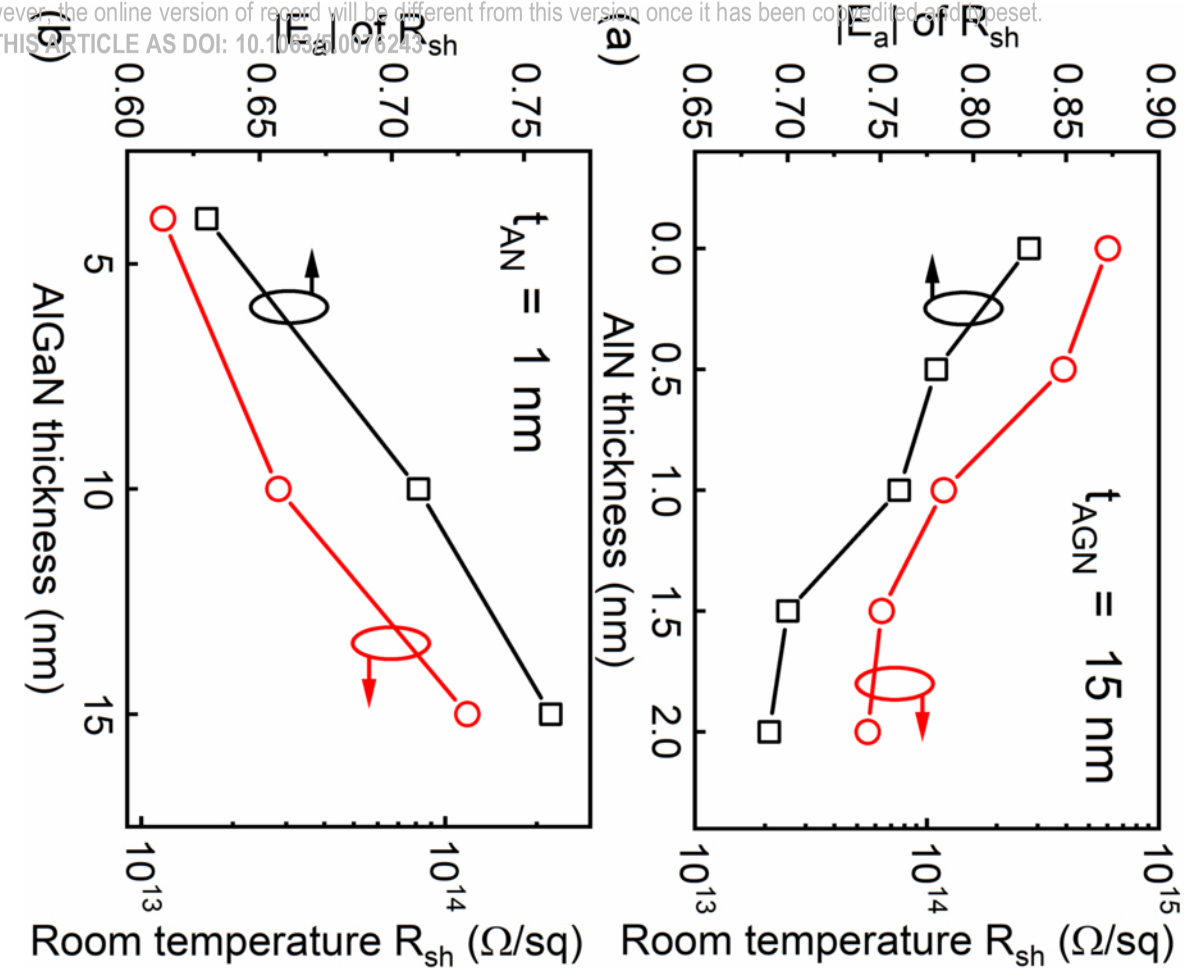

AIP Publishing

Journal of Applied Physics

ACCEPTED MANUSCRIPT

This is the author's peer reviewed, accepted manuscript. However, the online version of record will be different from this version once it has been copyedited and typeset.

PLEASE CITE THIS ARTICLE AS DOI: 10.1063/5.0076243

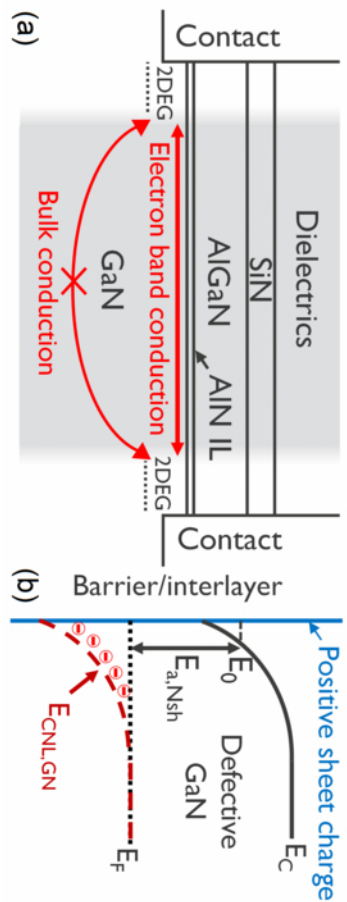

AIP Publishing

Journal of Applied Physics

ACCEPTED MANUSCRIPT

This is the author's peer reviewed, accepted manuscript. However, the online version of record will be different from this version once it has been copyedited and typeset.

PLEASE CITE THIS ARTICLE AS DOI: 10.1063/5.0076243

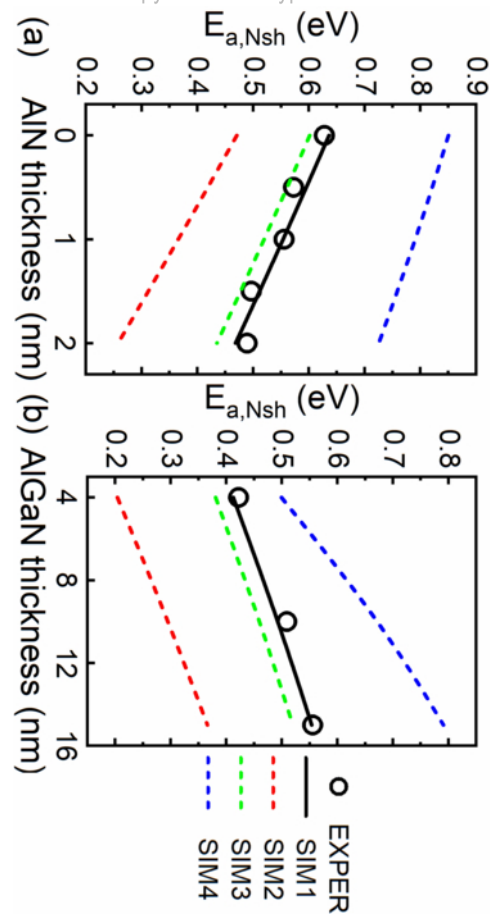

ACCEPTED MANUSCRIPT

Journal of Applied Physics

This is the author's peer reviewed, accepted manuscript. However, the online version of record will be different from this version once it has been copyedited and typeset.
PLEASE CITE THIS ARTICLE AS DOI: 10.1063/5.0076243